European Journal of Mechanics B/Fluids 28 (2009) 328–334

Contents lists available at ScienceDirect

European Journal of Mechanics B/Fluids

www.elsevier.com/locate/ejmflu

An analysis on the dependence on cross section geometry of galloping stability of two-dimensional bodies having either biconvex or rhomboidal cross sections

Gustavo Alonso *, Eusebio Valero, José Meseguer

IDR/UPM, E.T.S.I. Aeronáuticos, Universidad Politécnica de Madrid, E-28040 Madrid, Spain

ARTICLE INFO

Article history:
Received 22 February 2008
Received in revised form 30 July 2008
Accepted 30 September 2008
Available online 9 October 2008

Keywords:
Galloping
Cross-section geometry
Wind tunnel

ABSTRACT

Galloping is a well-known type of aeroelastic instability, but still difficult to predict as the relevant experimental data must first be obtained. Available information on non-rectangular cross-sections is scarce and non-systematic. The purpose of the present paper is to add new information gathered through static wind tunnel experiments. The effects of cross-sectional shape on the transverse galloping stability (according to the Glauert–Den Hartog criterion for galloping instability) of biconvex and rhomboidal cross-section bodies have been systematically analyzed. Measuring the aerodynamic coefficients and the pressure distributions along the body surfaces permits a better understanding of the galloping phenomenon and how the aerodynamic characteristics of the bodies evolve when changing parametrically the cross-section geometry from the known-case of the flat plate to the also known square or circular prisms. As a result of these investigations the potential unstable zones in the angle of attack – cross-section aspect ratio plane $(\alpha, t/c)$ are identified.

1. Introduction

Aeroelastic phenomena are becoming more and more important from the point of view of its potential application to modern structural design. Vortex shedding, translational galloping, wake galloping, torsional divergence, flutter and buffeting can be considered among these phenomena.

This paper is focused on the experimental analysis of translational galloping. As an aeroelastic phenomenon, galloping is caused by a coupling between the aerodynamic forces which act on a structure and the structural vibrations. Across-wind oscillation of the structure periodically changes the angle of attack of the incident wind. This variation in the angle of attack produces variation in the aerodynamic forces acting on the structure, and therefore produces variation in the response of the structure (Blevins [1]). Galloping instability conditions depend on a number of factors, such as the structure geometry and mechanical properties (mass, stiffness, damping) and the incident wind mean velocity, angle of incidence and turbulence.

Den Hartog explained for the first time galloping more than seventy years ago, introducing a very simple criterion for the stability of cross-wind oscillations: the quasi-static theory, which is an approximation to the analysis of the problem. At any moment in time, the aerodynamic forces experienced by an oscillating two-dimensional body are equivalent to that acting on a static two-dimensional body placed at different angles of incidence, assuming that the movement is quasi-steady. The Glauert–Den Hartog criterion for galloping instability states that for a given orientation of the body, α, assuming the variation of the angle of attack due to lateral oscillation around α is small enough, galloping instability can appear provided that:

$$\left(\frac{dc_l}{d\alpha_l} + c_d\right)\Big|_{\alpha_l=\alpha} < 0, \tag{1}$$

where $c_l = 2l/(\rho U^2 b)$ is the section lift coefficient, $c_d = 2d/(\rho U^2 b)$ the section drag coefficient and α the angle of attack; l and d are the aerodynamic forces, lift and drag, respectively, ρ the fluid density, U the upstream flow velocity and b is a cross-flow characteristic length of the body under consideration.

Eq. (1) is obtained after linearization of the equilibrium equation of the aerodynamic forces acting in the direction normal to the incident wing, and is closely related to the sign of the lift coefficient slope. Negative values of such slope may lead to potentially unstable situations. Galloping instability is explained because of the flow pattern around the body. In the situation of non-separated flow, as the angle of attack grows the lift coefficient grows accordingly, hence the lift slope becomes generally positive and galloping does not occur. However, if the angle of attack increases beyond a threshold value, the boundary layer separates and then the lift coefficient decreases. Therefore, in the situation of fully separated flow the lift coefficient slope becomes negative and according to Eq. (1) the possibility of galloping oscillations appears. Obviously, since the upstream turbulence may influence the reattachment,

* Corresponding author. Tel.: +34 91 33 66 353; fax: +34 91 33 66 363.
E-mail address: gustavo.alonso@upm.es (G. Alonso).

0997-7546/$ – see front matter
doi:10.1016/j.euromechflu.2008.09.004

this upstream turbulence may play a significant role in galloping phenomena.

In the last decades large efforts have been devoted to experimentally study the galloping features of many bodies having different cross-sections [2–4]. One of the reasons that support such studies is that some buildings and other slender structural elements are built more and more frequently with new techniques involving weigh-saving materials (reducing therefore the overall stiffness) and including innovative cross-sectional geometries. In consequence, when designing certain structures such as high and slender buildings or slender facade elements (like movable sunshade devices), critical velocities of aeroelastic instabilities such as vortex induced excitation and galloping can be found within design wind speed range.

However, most of the effort in galloping oscillation research has been concentrated in bodies with square or rectangular cross-sections, although prismatic bodies with other cross-sectional shapes may also be unstable to transverse galloping, as it happens with D-shaped cylinders, as well as highly asymmetric shapes such as ice-coated power lines and cables [5,6]. It is obvious that circular cylinders are not susceptible to galloping-induced vibrations at any angle of attack because of their symmetry ($\mathrm{d}c_l/\mathrm{d}\alpha_l = 0$).

A general analysis based on the Glauert–Den Hartog criterion of two-dimensional triangular cross-sectional bodies (the main vertex angle β ranging from 10° to 90°) can be found in Alonso and Meseguer [7], and a similar study based on dynamic tests is reported in [8,9], although this latter one is limited to the range $10° \leqslant \beta \leqslant 60°$. With dynamic tests, where the model in the wind tunnel can oscillate, the reduced velocity at which the galloping stability is initiated can be determined. Static tests allow to analyze the possibility of galloping appearance according to the Glauert–Den Hartog criterion.

Flat plates aerodynamic characteristics have been investigated in the past [10,11]. At low angles of attack the lift coefficient can be estimated by $c_l = 2\pi\alpha$, and therefore its slope is positive, until the flat plate stalls, at about $\alpha = 8°$. There is a small region then where the lift coefficient decreases, until $\alpha \cong 15°$, as flow separates from the upper surface, and from there c_l increases again moderately up to $\alpha \cong 40°$. For angles of attack $\alpha > 40°$ the lift coefficient decreases again, being obviously $c_l = 0$ for $\alpha = 90°$. In the first region where the lift coefficient slope is negative, the drag coefficient is still small, therefore between approximately $\alpha = 8°$ and $\alpha \cong 15°$ the flat plate shows galloping instability. There is a second angle of attack interval with negative c_l curve slope, at $40° < \alpha < 90°$, but there the value of c_d is really large and therefore galloping does not appear.

Square cylinders behavior is also very well known, both theoretically and experimentally (Kazakevich and Vasilenko [12]). Instability is possible for $-30° < \alpha < 60°$, the reference $\alpha = 0°$ corresponding to incident flow perpendicular to the windward side of the square.

Based on these known results, the aim of the investigations reported in this paper is to better understand the dependence of the galloping instability on the cross section geometry of two different types of cylinders: biconvex and rhomboidal (upper and lower surfaces of biconvex profile are both equal arch of circumference).

In the case of a biconvex cylinder having a cross section of chord c and thickness t (Fig. 1), if the aspect ratio $\tau = t/c$ is very small, the behavior of the body will be very similar to that of a flat plate, therefore it will show galloping oscillations for angles of attack close to the interval $8° \leqslant \alpha \leqslant 15°$, which is the one corresponding to the flat plate. On the other hand, if the aspect ratio is now increased up to $\tau = 1$, the cross section shape becomes a circle, which does not gallop because of the symmetry, since the lift coefficient of a circular cylinder does not change with the angle of attack. Different biconvex cross sections with the same chord c and aspect ratios ranging from $\tau = 0.183$ to $\tau = 0.839$ have been tested to clarify where galloping instability appears.

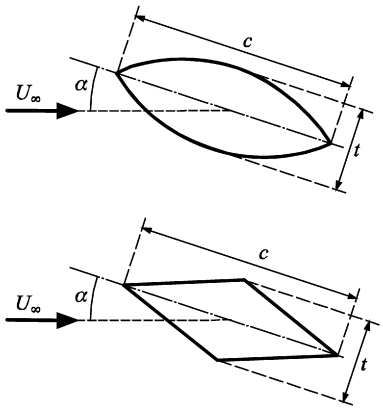

Fig. 1. Definition of both the biconvex cross-section bodies and the rhomboidal cross-section bodies used in galloping experiments.

Another interesting transition from a flat plate to a known result can be obtained with rhomboidal cross sections. For a given chord c (the long diagonal) increasing the size of the thickness t (the short diagonal) from $\tau = t/c = 0$ to $\tau = 1$, transition from a flat plate to a square cylinder is obtained (Fig. 1). Both flat plates and squares gallop (at certain angles of attack). Therefore intermediate rhomboidal profiles could be expected to show a similar behavior. The interest is then to determine which are the regions in the (α, τ) plane where galloping instability takes place.

In this paper the stability to cross-flow translational galloping vibration of biconvex and rhomboidal two-dimensional cross-section bodies, with varying aspect ratios and angles of attack ranging from $\alpha = 0°$ to $\alpha = 90°$, has been analyzed through wind tunnel experiments. Experimental configurations and tests procedures are described in next section. Results are presented in Section 3 and, finally, conclusions are outlined in Section 4.

2. Experimental set-up

Galloping stability analysis has been performed according to standard procedures usually followed in galloping studies. As it has been stated above, the main objective of this work is to examine the effects of cross-sectional shape and mean wind angle of incidence on the transverse galloping stability of different cross-section bodies. Since the sign of the function $H(\alpha) = \mathrm{d}c_l/\mathrm{d}\alpha + c_d$ determines the stability of the body to transverse galloping (the obstacle could gallop provided that $H(\alpha)$ is negative), information on $\mathrm{d}c_l/\mathrm{d}\alpha$ gives a first approximation to galloping instability.

Aerodynamic coefficients, lift and aerodynamic drag, were measured in an open circuit two-dimensional wind tunnel, using rigidly mounted configurations. Wind tunnel test chamber is 0.15 m width, 0.90 m high and 1.20 m long. Wind velocity profile at the model test section is uniform within ±1%, the turbulence intensity being around 4%. The wind velocity of the stream at the test section of the wind tunnel was 25 $\mathrm{m\,s^{-1}}$, which provides Reynolds numbers based on the model characteristic length, c, of $Re = 2.2 \times 10^5$ for the biconvex profiles ($c = 0.125$ m), and $Re = 1.3 \times 10^5$ for the rhombi ($c = 0.075$ m).

Aerodynamic loads were measured with a six-component strain-gauge balance (ATI, model Gamma SI-130-10). The balance is mounted on a fixed reference frame in such a way that one of the balance axes becomes aligned with the upstream direction. The balance supports a rotating platform to which the model is fixed through an appropriated screw. The rotating platform allows setting the model angle of attack with ±0.5° accuracy. The balance has a maximum measurement uncertainty of 1.25%.

Six biconvex cross-section prisms were tested, the aspect ratio being $\tau = 0.183$, 0.344, 0.504, 0.667, 0.742 and 0.839. The models span is 0.145 m. Concerning rhombi, eight different prisms were tested, with aspect ratio $\tau = 0.194$, 0.252, 0.329, 0.357, 0.460, 0.580, 0.799 and 1.000. The models span is also 0.145 m. It must be pointed out that measurements have been corrected by using usual wind tunnel correction methods to take into account test chamber blockage because of the model (Barlow, Rae and Pope [13]).

Once a selected model is fixed to the rotating platform, and the initial angle of attack is set, the experimental sequence runs almost automatically. Angles of attack are varied from $\alpha = 0°$ to $\alpha = 90°$ at 2° steps, and at each step the lift and drag outputs coming from the balance are stored in a PC, amongst other signals, for further analysis. Static and dynamic pressures inside the test chamber were measured with an Air Flow 048 Pitot tube connected to a Schaewitz Lucas P-3061-2WD pressure transducer.

Concerning biconvex profiles, an interesting transition in the aerodynamic characteristics of this type of bodies takes places at an aspect ratio of $\tau = 0.839$: at high angles of attack a sudden change of the lift coefficient sign occurs, so that the lift coefficient drops from moderate positive values ($c_l \cong 0.3$) to negative ones ($c_l \cong -0.3$). In all the tested bodies there are two regions in the $c_l(\alpha)$ curve where the slope $\mathrm{d}c_l/\mathrm{d}\alpha$ becomes negative. These two regions collapse in a single one as τ grows in the case of rhombi, but in biconvex profiles the second region where $\mathrm{d}c_l/\mathrm{d}\alpha < 0$ becomes steeper as the aspect ratio τ increases and finally disappears as the body cross section approaches the circular shape ($\tau = 1$). Since galloping instability is known to be related to the flow morphology around the body, another set of experiments has been run in order to measure pressure distributions on the surfaces of a biconvex body with $\tau = 0.839$. These tests have been run in a two-dimensional, open circuit wind tunnel, whose test chamber is 0.20 m width, 1.80 m high and 1.50 m long. Wind velocity profile at the model test section is uniform within ±1%, the turbulence intensity being around 3%. The wind velocity of the stream at the test section of the wind tunnel was 30 $\mathrm{m\,s^{-1}}$, and the model chord, $c = 0.19$ m, so that Reynolds number was close to $Re = 4 \times 10^5$.

In order to measure the pressure distribution on the surfaces of the biconvex cross-section prisms, a total of 29 pressure taps uniformly distributed along one of the surfaces of the prism were drilled with a separation of 10 mm between taps (the first tap being located at 5 mm from the section leading edge). A pressure scanner from Scanivalve Corp. was attached therein; with this pressure scanner up to 126 pressure signals can be sampled almost simultaneously. The pressure signal (sampling frequency of 20 Hz) was sent to a personal computer. A total of 250 pressure signals at each location were time-averaged to obtain the local pressure coefficient.

With this experimental set up pressures have been measured on the biconvex prism with $\tau = 0.839$ for angles of incidence α ranging from 0° to 90°, in 5° steps.

3. Results and discussion

The variation with the angle of incidence of both aerodynamic coefficients (c_l and c_d) as well as the function $H(\alpha) = \mathrm{d}c_l/\mathrm{d}\alpha + c_d$ is shown in Fig. 2 in the case of rhomboidal profiles, and in Fig. 4

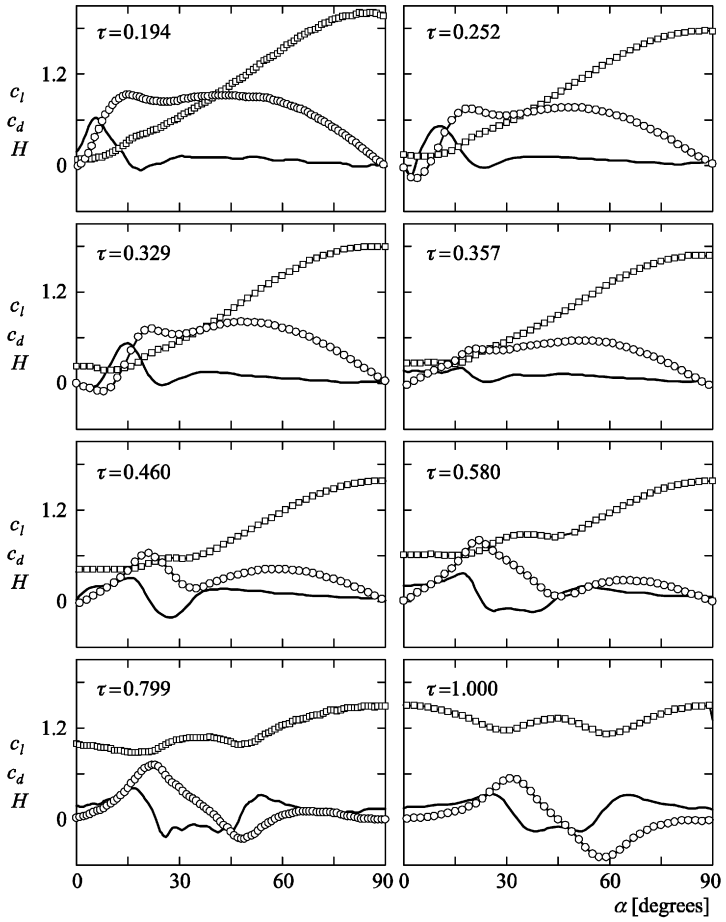

Fig. 2. Variation with the angle of attack α of the lift coefficient c_l (circles), the aerodynamic drag c_d (squares) and the function $H = \mathrm{d}c_l/\mathrm{d}\alpha + c_d$ (continuous line), for several rhomboidal cross-section bodies having different aspect ratio τ.

in the case of biconvex profiles. In both cases results are presented for the range $0° \leqslant \alpha \leqslant 90°$ (obviously the lift force curves are antisymmetric with respect to both $\alpha = 0°$ and $\alpha = 90°$, whereas the drag force ones are symmetric with respect to these values, $\alpha = 0°$ and $\alpha = 90°$).

Small aspect ratio rhomboidal profiles ($\tau = 0.194$) behave very similar to flat plates, where two zones with negative lift slope can be found, the first one close to $\alpha = 8°$, where the flat plate stalls, and the second for $\alpha > 40°$, as already stated. This second negative lift slope zone occurs because there is not circulation on the plate and the whole upper surface is stalled, then, although the normal to the plate force coefficient c_n increases with the angle of attack, its projection on a direction perpendicular to the incident flow (the lift coefficient, $c_l = c_n \cos\alpha$) decreases (Wick [10]). In any case, in this interval of high values of the angle of attack, the flat plate is not prone to gallop because the drag coefficient is large, so that $H(\alpha) = \mathrm{d}c_l/\mathrm{d}\alpha + c_d$ is positive, hence the only possibility of galloping takes place when the plate stalls after boundary layer detachment ($8° \leqslant \alpha \leqslant 15°$). As the aspect ratio increases, approximately from $\tau = 0.252$, a third region of negative slope appears just from $\alpha = 0°$ (see the results corresponding to $\tau = 0.252$ and $\tau = 0.329$ in Fig. 2). Increasing from there slightly the aspect ratio, just to $\tau = 0.357$ shows how that zone of negative slope close to $\alpha = 0°$ vanishes, and the two remaining zones with negative lift slope get softened and almost disappear, so does the galloping instability of that geometrical configuration.

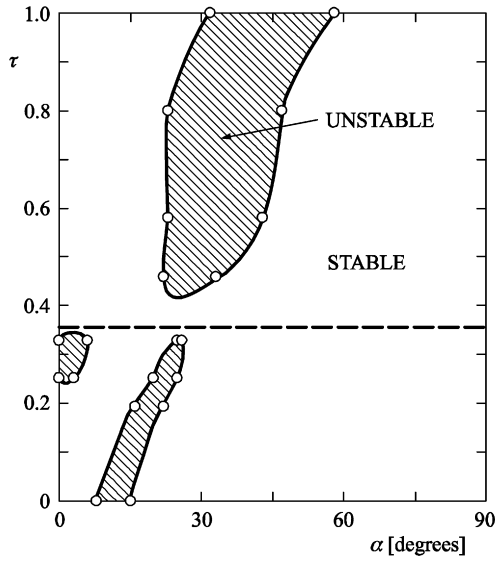

Fig. 3. Stability diagram in the angle of attack – aspect ratio plane (α, τ), based on static test results, of the galloping of rhomboidal cross-section bodies. Symbols represent the stability boundaries $H = \mathrm{d}c_l/\mathrm{d}\alpha + c_d = 0$ for the corresponding aspect ratio according to the static Glauert–Den Hartog criterion. The dashed line corresponds to the case $\tau = 0.357$ which is stable no matter the value of the angle of attack is.

The pattern changes for still higher aspect ratio cross sections (from $\tau = 0.460$ to $\tau = 0.799$). Now there is only one zone with a high enough negative lift slope value so that galloping can develop, along a wide interval of angles of incidence. Finally the square section ($\tau = 1.000$) shows the same behavior with the expected symmetry. All these results are summarized in Fig. 3, where the galloping stability/instability regions in the (α, τ) plane according to the Glauert–Den Hartog criterion are shown. Two main zones of potential instability can be identified in that stability map taken into account the sign of $H(\alpha)$. A first zone fills in a narrow region corresponding to small values of τ showing an almost linear dependency of unstable values of τ with α. That means that in this region the angle of incidence at which a given rhomboidal profile is unstable grows as the aspect ratio of the profile increases, starting around $\alpha = 12°$ for the flat plate up to $\alpha = 25°$ for $\tau < 0.357$. After a discontinuity around $\tau = 0.357$ a new unstable region appears, from $\tau \cong 0.450$ to $\tau = 1.000$, the intervals of angles of attack where rhombi can gallop being wider as the aspect ratio grows.

When biconvex profiles are considered, also in this case small aspect ratio profiles ($\tau = 0.183$) behave very similar to flat plates.

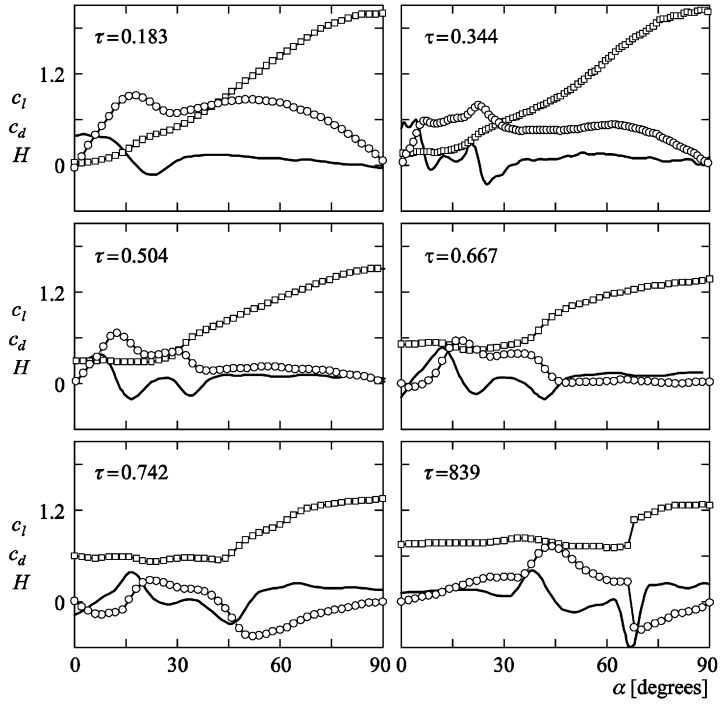

Fig. 4. Variation with the angle of attack α of the lift coefficient c_l (circles), the aerodynamic drag c_d (squares) and the function $H = \mathrm{d}c_l/\mathrm{d}\alpha + c_d$ (continuous line), for several biconvex cross-section bodies having different aspect ratio τ.

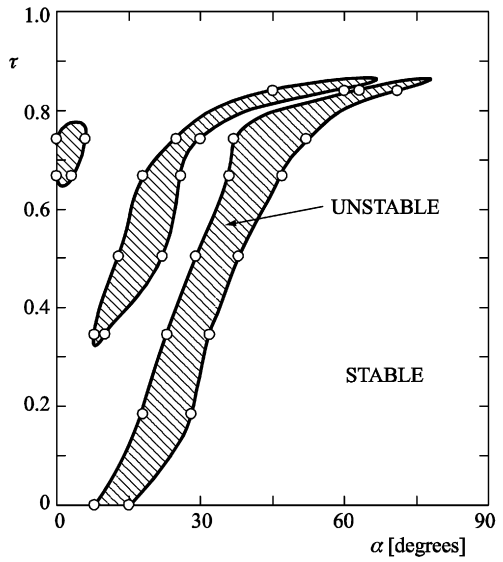

Fig. 5. Stability diagram in the angle of attack – aspect ratio plane (α, τ), based on static test results, of the galloping of biconvex cross-section bodies. Symbols represent the stability boundaries $H = \mathrm{d}c_l/\mathrm{d}\alpha + c_d = 0$ for the corresponding aspect ratio according to the static Glauert–Den Hartog criterion.

As the aspect ratio increases ($\tau = 0.344$ and $\tau = 0.504$) there are two zones where the lift slope is negative and the drag coefficient is not large enough to avoid galloping instability (Fig. 4). For angles of incidence small enough and small aspect ratio ($\tau = 0.344$) the lift coefficient grows as α grows, although boundary layer separation near the leading edge takes place for small values of α. However, the shear layer reattaches on the body upper side and a recirculation bubble is formed close to the leading edge. Note that although biconvex profiles have a curvilinear shape they have also sharp edges, therefore the separation point is generally fixed at any of the sharp edges and the effect of the Reynolds number is not very important in this case. As the angle of incidence grows separation occurs at the leading edge and the reattachment point moves towards the trailing edge, so that in this range of values of the angle of incidence the lift still increases as α grows. This behavior ends when the reattachment point reaches a certain point on the body upper side. Beyond this angle of attack reattachment is no longer possible, therefore for further increments of α, the variation of the lift coefficient corresponds to a fully detached flow similar to the one described for the rhombi case. Thus there are three maxima in the lift coefficient curve and consequently three intervals of the angle of attack where the lift slope is negative, although galloping can develop only where aerodynamic drag is no too large. As τ grows the first maximum of the lift curve increases whereas the second decreases and the third practically disappears (as it is the case of $\tau = 0.504$ in Fig. 4).

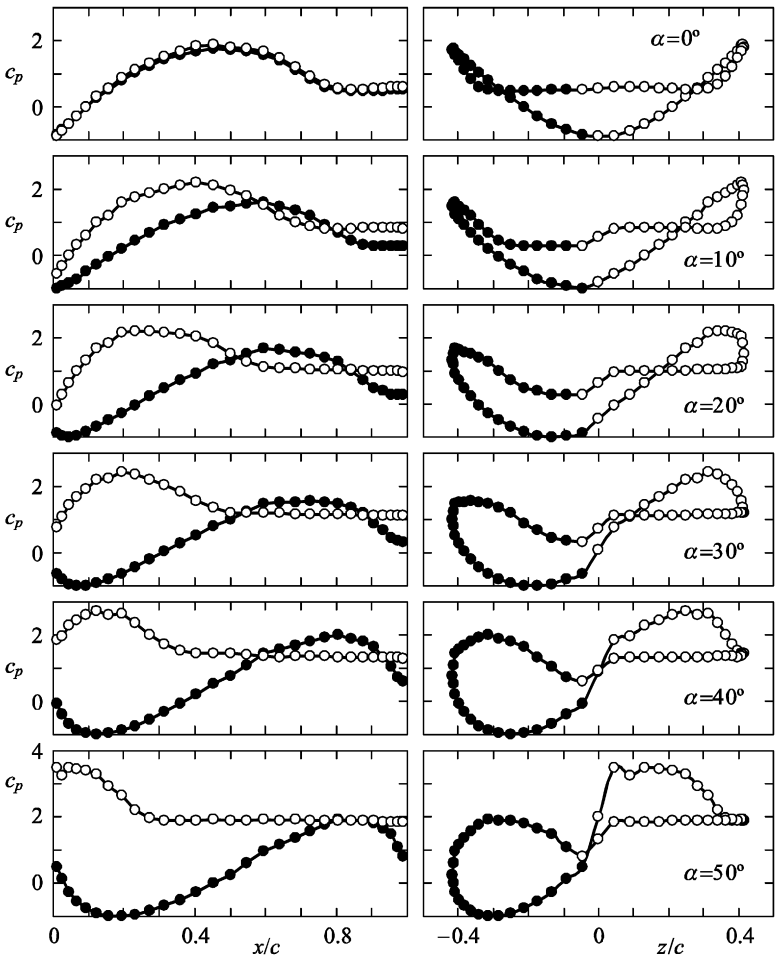

Fig. 6. Pressure coefficient distributions along the body axes measured on the surfaces of a biconvex cross-section body with an aspect ratio $\tau = 0.839$ for angles of attack α ranging from 0° to 90°.

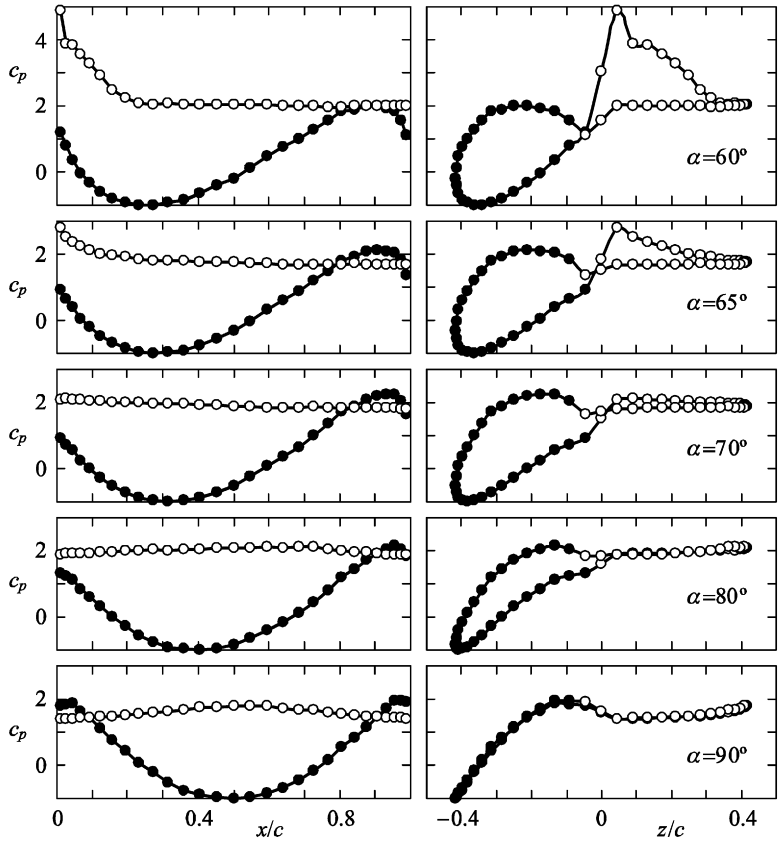

Fig. 6. (*continued.*)

The pattern changes for still higher values of the aspect ratio ($\tau = 0.667$ and $\tau = 0.742$). Now the third peak corresponding to large values of the angle of attack does not exists and the second one vanishes as τ grows, although there are still two regions where the lift slope is negative. In addition a new zone with negative lift slope appears, right at $\alpha = 0°$ (Fig. 5). This new zone also disappears as the aspect ratio increases, while the negative slope zone corresponding to medium values of the angle of attack becomes steeper and moves to higher values of α (the lift coefficient becomes even negative in spite of the angle of attack is positive). Very high aspect ratio biconvex profile, $\tau = 0.839$, shows two zones where the lift slope is negative, being the second one amazingly sharp: the lift coefficient changes sign, almost keeping its absolute value in just two degrees, between $\alpha = 66°$ and $\alpha = 68°$.

Taking into account the sign of the function $H(\alpha) = \mathrm{d}c_l/\mathrm{d}\alpha_0 + c_d$ defining the Glauert–Den Hartog criterion for galloping instability, the different unstable zones in the plane (α, τ) have been represented in Fig. 5, where three main zones of potential instability are identified. A first zone fills in a narrow band of angles of attack which is approximately 10°, with an almost linear dependence of τ with α. That means that in this region the angle of incidence at which a given biconvex profile is unstable grows as the aspect ratio of the profile increases, starting at $\alpha \cong 12°$ for the flat plate up to $\alpha = 50°$ for $\tau \cong 0.80$. From there, the slope of this instability region becomes smaller and finally the unstable zone dies, being the circular profile ($\tau = 1$) stable for any value of α. A second instability zone appears at intermediate aspect ratio cross sections, between $\tau = 0.34$ and $\tau = 0.75$, also with a linear relationship of τ with α, and in a 10° interval. The slope of such second instability zone also changes for high enough aspect ratios, vanishing when this parameter approaches the value $\tau = 1$. Finally, high aspect ratio profiles ($\tau = 0.667$ and $\tau = 0.742$) show a third instability region around $\alpha = 0°$.

In order to explain the jump of the lift coefficient appearing in high aspect ratio biconvex profiles the pressure coefficient on a biconvex profile with $\tau = 0.839$ has been measured for angles of incidence from $\alpha = 0°$ to $\alpha = 90°$ varying the angle of attack in 5° steps. The results corresponding to some selected angles of attack are shown in Fig. 6, where the variation of the pressure coefficient with both the x coordinate and the z coordinate have been represented; (x, z) are body axes, the origin is placed at the profile leading edge for $\alpha = 0°$, x axis coincides with the profile chord whereas z axis is perpendicular to the chord. With this representation of pressure distributions, the area enclosed by the experimental data directly gives either the normal to chord force coefficient, c_n, or the tangential to the chord force coefficient, c_t:

$$c_n = \frac{1}{c}\int_0^c (c_{p,l} - c_{p,u})\,\mathrm{d}x, \tag{2}$$

$$c_t = \frac{1}{c}\int_0^c (c_{p,w} - c_{p,t})\,\mathrm{d}z, \tag{3}$$

where the subscripts l and u in Eq. (2) mean lower and upper surface of the biconvex profile, respectively, and the subscripts w and t in Eq. (2) mean windward and leeward sides of the profile, and identify the part of the profile between the leading edge and the maximum thickness and the part spanning between that point and the trailing edge, respectively. Note that with this representation a given pressure distribution can draw one or several loops which represent negative or positive forces in the body axes system (obviously pressure forces acting on the leading edge side of the profile generate thrust, whereas those of the trailing edge gen-

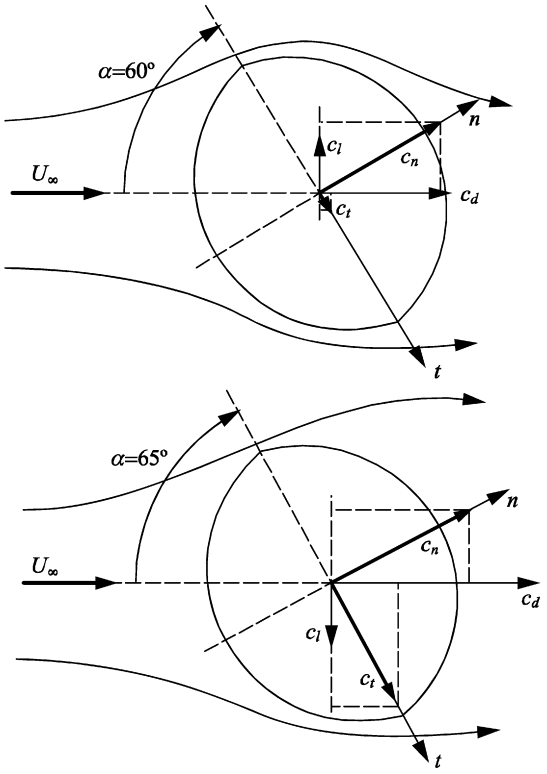

Fig. 7. Sketch of the flow configuration and the force coefficients on a biconvex profile with $\tau = 0.839$ at $\alpha = 60^\circ$ and $\alpha = 65^\circ$.

erate drag). Once c_n and c_t are known, the lift and pressure drag coefficients are

$$\left.\begin{aligned} c_l &= c_n \cos\alpha - c_t \sin\alpha \\ c_d &= c_n \sin\alpha + c_t \cos\alpha \end{aligned}\right\}. \tag{4}$$

According to the results depicted in Fig. 6 at small values of the angle of attack the flow is attached in a wide zone spanning from the leading edge till $x/c \approx 0.8$. As the angle of attack increases such upper side separation point moves towards the leading edge whereas that of the lower side moves towards the trailing one. However, at the upper side the boundary layer also separates at the leading edge (the boundary layer is still laminar when it reaches the leading edge), appearing then a separation bubble that reattaches at a certain point on the body upper side. This separation bubble and the subsequent reattachment followed by the second separation is clearly shown in the experimental data when $\alpha > 20^\circ$ (the reattachment point is identified by a small rut in the upper side pressure distribution). The size of the leading edge separation bubble decreases as α increases, causing a remarkable suction peak at the leading edge for $\alpha \approx 60^\circ$. Obviously the region where boundary layer is not separated after the reattachment decreases as the angle of attack grows, but even at $\alpha \approx 60^\circ$ the boundary layer does not separates until $x/c \approx 0.2$. If the angle of attack is slightly increased, the flow does not reattach any more, the separation bubble disappears, and the whole profile upper side becomes stalled (so that c_n notably decreases).

On the body lower side, the stagnation points moves as the angle of attack grows, from the leading edge at $\alpha = 0^\circ$ to the middle of the side at $\alpha = 90^\circ$, which is a logical result given the symmetry of the configuration.

Concerning the tangential force c_t, experimental results in Fig. 6 show that this force is larger when the boundary layer separates, as one could expect, with a sudden increase when the separation bubble disappears (note that for $\alpha = 65^\circ$ the suction loop practically collapses). Taking into account the behavior of both c_n and c_t close to $\alpha = 60^\circ$ the variation of the lift coefficient c_l and the drag coefficient c_d are easily explained (Fig. 7) in view of expressions (4); at such high value of the angle of attack the lift coefficient depends mainly on the value of c_t, so that a sudden increase of this tangential coefficient can even change the sign of the lift and give a valuable increase of the drag coefficient.

4. Conclusions

The work reported in this paper shows the progress that has been made on the understanding of the transverse galloping instability. The galloping stability of two different geometries, rhomboidal and biconvex profiles, has been studied by means of wind tunnel tests following the Glauer–Den Hartog criterion. It has been proved that the stability to transverse galloping stability of those cross-section cylinders is, as expected, angle of attack dependent, and the influence of the aspect ratio has been identified and related to the flow pattern around the body.

Stability maps in the angle of attack – aspect ratio plane have been presented both for rhomboidal and biconvex cross sections. From them can be observed how rhomboidal cross sections profiles evolve from a flat plate like behavior for small aspect ratios and maintain an instability region as the aspect ratio increase up to the square case, but with a short discontinuity for aspect ratios about $\tau \cong 0.36$, which are stable in the whole angle of attack range.

On the other hand, biconvex profiles evolve from a flat plate like behavior when they have a small aspect ratio, maintaining an instability zone at any aspect ratio up to close the circular cylinder ($\tau = 1$) when obviously the instability disappears. Biconvex profiles are particularly prone to gallop at relatively high values of the aspect ratio (say $0.65 \leqslant \tau \leqslant 0.85$) when they are subjected to high angle of attack flows.

References

[1] R.D. Blevins, Flow Induced Vibration, second ed., Krieger Publishing Company, Malabar, 2001.
[2] H. Ruecheweyh, M. Hortmanns, C. Schnakenberg, Vortex-excited vibrations and galloping of slender elements, J. Wind Eng. Ind. Aerodyn. 65 (1996) 347–352.
[3] H. Kawai, Effect of corner modifications on aeroelastic instabilities of tall buildings, J. Wind Eng. Ind. Aerodyn. 74-76 (1998) 719–729.
[4] S.C. Luo, Y.T. Chew, T.S. Lee, M.G. Yazdani, Stability to translational galloping vibration of cylinders at different mean angles of attack, J. Sound Vib. 215 (1998) 1183–1194.
[5] O. Chabart, J.L. Lilien, Galloping of electrical lines in wind tunnel facilities, J. Wind Eng. Ind. Aerodyn. 74-76 (1998) 967–976.
[6] P. McComber, A. Paradis, A cable galloping model for thin ice accretions, Atmos. Res. 46 (1998) 13–25.
[7] G. Alonso, J. Meseguer, A parametric study of the galloping instability of triangular cross-section bodies, J. Wind Eng. Ind. Aerodyn. 94 (2006) 241–253.
[8] G. Alonso, J. Meseguer, I. Pérez-Grande, Galloping oscillations of two-dimensional triangular cross-sectional bodies, Exp. Fluids 38 (2005) 789–795.
[9] G. Alonso, J. Meseguer, I. Pérez-Grande, Galloping stability of triangular cross-sectional bodies: A systematic approach, J. Wind Eng. Ind. Aerodyn. 95 (2007) 928–940.
[10] B.H. Wick, Study of the subsonic forces and moments on an inclined plate of infinite span, NACA TN 3221, NACA, Washington, 1954.
[11] R.D. Blevins, Applied Fluid Dynamics Handbook, Krieger Publishing Company, Malabar, 1992.
[12] M.I. Kazakewich, A.G. Vasilenko, Closed analytical solution for galloping aeroelastic self-oscillations, J. Wind Eng. Ind. Aerodyn. 65 (1996) 353–360.
[13] J.B. Barlow, W.H. Rae, A. Pope, Low-Speed Wind Tunnel Testing, John Wiley & Sons, Inc., New York, 1999.